Inorg. Chem. **2008**, *47*, 5601−5611

Lanthanide-Centered Covalently Bonded Hybrids through Sulfide Linkage: Molecular Assembly, Physical Characterization, and Photoluminescence

Bing Yan*,†,‡ and Hai-Feng Lu†

Department of Chemistry, Tongji University, Shanghai 200092, China, and State Key Laboratory of Rare Earth Materials Chemistry and Applications, Beijing 100871, China

Received November 6, 2007

A series of novel photoactive lanthanide (europium, terbium, dysprosium, samarium) hybrid materials with organic parts covalently bonded to inorganic parts via sulfide linkage have been assembled by the sol−gel process. The organic parts as molecular bridge are obtained from the functionalized thiosalicylic acids by five silane crosslinking reagents, 3-chloropropyltrimethoxysilane, 3-methacryloyloxypropyltrimethoxysilane, 3-aminopropyltrimethoxysilane, 3-glycidoxypropyltrimethoxysilane, and 3-(triethoxysilyl)propylisocyanate. The intramolecular energy transfer process between lanthanide ions and the molecular bridges took place within these molecular-based hybrids and especially the quantum efficiency of europium hybrids were determined, suggesting that the hybrid material systems derived from different molecular bridges present different luminescence efficiencies.

Introduction

Organic−inorganic hybrid materials have been widely studied in the past two decades.[1] These systems provide the opportunity to produce many innovative advanced materials, which present improved physical and chemical properties, as well as the promising applications in many fields such as optics, electronics, mechanics, membranes, protective coatings, catalysis, sensors, biology, and so forth.[2] Luminescent materials are applied in many important optical devices of tunable lasers, displays, and amplifiers for optical communication.[3] Many lanthanide complexes have been investigated extensively, owing to their long-lived excited-states characters and their especially efficient strong narrow-width emission band in the visible region.[4] So, entrapping rare-earth complexes with β-diketones, aromatic carboxylic acids, and heterocyclic ligands in sol−gel-derived host materials has been studied to improve the thermal stability and mechanical property of the lanthanide complexes.[4–7]

The sol−gel process allows the preparation of silica-based or siloxane-based materials doped with lanthanide complexes by hydrolysis and polymerization of silicon alkoxides at ambient temperatures.[8,9] The resulting materials are transparent and have good mechanical properties such as high sample homogeneity and purity.[1] But the solubility of lanthanide complexes in the sol−gel matrix is low as a result of the low pH needed for the hydrolysis reaction.[9,10] Some methods have been put forward to overcome these solubility problems such as introducing organic components into the material.[2,11] The properties of those inorganic−organic hybrid materials depend on the chemical nature of the different constituents. This is known to be class I hybrid materials for which only weak interactions (typically hydrogen bonds or van der Waals forces) exist between organic and inorganic parts.[12] The luminescence of these materials is hampered by the quench-

* To whom the correspondence should be addressed. Email: byan@tongji.edu.cn. Fax: +81-21-65982287. Phone: +81-21-65984663.
† Tongji University.
‡ State Key Laboratory of Rare Earth Materials Chemistry and Applications.

(1) Schubert, U.; Husing, N.; Lorenz, A. *Chem. Mater.* **1995**, *7*, 2010.
(2) Sanchez, C.; Sloer-Illia, G. J. D. A.; Ribot, F.; Lalot, T.; Mayer, C. R.; Cabuil, V. *Chem. Mater.* **2001**, *13*, 3061.
(3) Blasse, G.; Grabmaier, B. C. *Luminescent Materials*; Springer, Berlin, 1994.
(4) Matthews, L. R.; Knobbe, E. T. *Chem. Mater.* **1993**, *5*, 1697.
(5) Yan, B.; Zhang, H. J.; Ni, J. Z. *J. Photochem. Photobiol. A Chem.* **1998**, *112*, 231.
(6) Zhang, Y.; Wang, M.; Xu, J. J. *Mater. Sci. Eng.* **1997**, *B47*, 23.
(7) Serra, O. A.; Nassa, E. I.; Zapparolli, G.; Rosa, I. L. V. *J. Lumin.* **1997**, *72*, 263.
(8) Brinker, C. J.; Scherer G. W. *Sol-Gel Science*, Academic Press: San Diego, CA, 1990.
(9) Driesen, K.; Gorller-Walrand, C.; Binnemans, K. *Mater. Sci. Eng.* **2001**, *C18*, 255.
(10) Driesen, K.; Lenaerts, F.; Binnemans, K.; Gorller-Walrand, C. *Phys. Chem. Chem. Phys.* **2002**, *4*, 552.
(11) Sanchez, C.; Ribot, F. *New J. Chem.* **1994**, *18*, 1007.

10.1021/ic7021825 CCC: $40.75
Published on Web 05/28/2008

ing of the excited states via vibronic coupling with the hydroxyl group vibrations (in Si−OH and H_2O).[13–16] One way to decrease the concentration of hydroxyl groups is to calcine the sol−gel materials at high temperatures so as to decrease the degree of quenching. This way has been successfully demonstrated for sol−gel processed glasses, optical fibers, and thin films. But those materials have the low absorbance because the organic ligands are decomposed at the high calcination temperatures, and there is little energy transition between the host and the central ions.[13] Another way to avoid the quenching of the excited state is to link organic and inorganic parts together while shielding the lanthanide ion from the deactivating groups by a shell of organic ligands,[14] and this is called class II hybrid materials.[17–25] The organic ligands can reinforce the energy absorbability with chromophoric groups, and the energy can be transferred to the lanthanide ions efficiently. The inorganic composition can enhance thermal and mechanical resistances. In addition, the covalent Si−C bonds grafting the lanthanide complexes to the silica backbone make the final production monophasic even at a high concentration of organic chelates.[2] So the materials' properties are improved largely, and lanthanide-containing organic−inorganic hybrid materials processed by the sol−gel method are considered to be good candidates to be applied in optical devices.

Our recent work concerns the covalently bonded hybrids.[26–35] We have successfully realized three paths to construct lanthanide hybrid materials with chemical bonds. The first path is to modify the amino groups of organic ligands using 3-(triethoxysilyl)-propyl isocyanate (abbreviated as TESPIC) through the reaction between the amino group of ligands and intern ester group (isocyanate) of TESPIC, further assembling the above modified bridge ligands with lanthanide ions and inorganic precursors (TEOS) to hybrid systems.[26,27] The second path is to modify the carboxylate group of aromatic carboxylic acids through the amidation reaction between the carbonyl groups of acids and the amino group of amino-silane crosslinking reagents, then composing hybrid materials with covalent bonds.[28–30] The third path is to modify the hydroxyl group of organic ligands using TESPIC through the addition reaction between the hydroxyl group of ligands and intern ester group (isocyanate) of TESPIC, further assembling the above modified bridge ligands with lanthanide ions and inorganic precursors (TEOS) to hybrid systems.[31–34] On the basis of the above research, we can modify the two typical kinds of crosslinking reagents with different groups (TESPIC and 3-aminopropyl-methyldiethoxylsiliane) together through the hydrogen transfer addition reaction to form di-urea linkages between isocyanate and the amino groups and then design ternary hybrid materials with chemical bonding.[35] In view of these researches, it can be recognized that the key procedure to construct molecular-based materials is to design a functional bridge molecule by the grafting reaction, which can behave double functions of both coordinating to lanthanide ions and sol−gel processing to constitute a covalent Si−O network.[26–35] The development of novel linkages for connecting organic compounds to inorganic solid supports is an important and active field because the stability of the linkage limits the synthesis route and the property of the final material.[36] In the former research, many researchers have paid their attention to modification of the siloxanes, such as 3-aminopropyl trimethoxysilane,[37] 3-methacryloyloxypropyl trimethoxysilane,[38] 3-glycidoxypropyltrimethoxysilane,[39] and 3-(triethoxysilyl)propylisocyanate.[40]

In this article, a sulfide bond was selected to construct the linkage between inorganic and organic parts. It can react with 3-chloropropyl trimethoxysilane, 3-aminopropyl trimethoxysilane, 3-methacryloyloxypropyl trimethoxysilane, 3-glycidoxypropyltrimethoxysilane, and 3-(triethoxysilyl-)propyl isocyanate, respectively, and the derived multifunctional organosilane precursor could be utilized to coordinate to Eu^{3+}/Tb^{3+} ions respectively and to pass a sol−gel process to obtain the anticipant hybrid materials. In this way, numerous compounds containing sulfide linkages are expected to be introduced into the hybrids and more multifunctional luminescent materials could be obtained.

Experimental Section

Materials. Starting materials were purchased from Aldrich or Fluka and were used as received. All organic solvents were purchased from China National Medicines Group and were distilled

(12) Fujiyama, T.; Hori, M.; Sasaki, M. *J. Non-Cryst. Solids* **1990**, *121*, 273.
(13) Driesen, K.; Van Deun, R.; Gorller-Walrand, C.; Binnemans, K. *Chem. Mater.* **2004**, *16*, 1531.
(14) Viana, B.; Koslova, N.; Aschehoug, P.; Sanchez, C. *J. Mater. Chem.* **1995**, *5*, 719.
(15) Crosby, G.; Whan, R. E.; Alire, R. *J. Chem. Phys.* **1961**, *34*, 743.
(16) James, I. W. *Tetrahedron* **1999**, *55*, 4855.
(17) Li, H. R.; Lin, J.; Zhang, H. J.; Fu, L. S. *Chem. Mater.* **2002**, *4*, 3651.
(18) Li, H. R.; Lin, J.; Zhang, H. J.; Fu, L. S. *Chem. Commun.* **2001**, 1212.
(19) Dong, D. W.; Jiang, S. C.; Men, Y. F.; Ji, X. L.; Jiang, B. Z. *Adv. Mater.* **2000**, *12*, 646.
(20) Franville, A. C.; Zambon, D.; Mahiou, R. *Chem. Mater.* **2000**, *12*, 428.
(21) Sun, L. N.; Zhang, H. J.; Meng, Q. G.; Liu, F. Y.; Fu, L. S.; Peng, C. Y.; Yu, J. B.; Zheng, G. L.; Wang, S. B. *J. Phys. Chem. B.* **2005**, *109*, 6174.
(22) Ferreira, R. A. S.; Carlos, L. D.; Goncalves, R. R.; Ribeiro, S. J. L.; Bermudez, V. D. Z. *Chem. Mater.* **2001**, *13*, 2991.
(23) Carlos, L. D.; Ferreira, R. A. S.; Pereira, R. N.; Assuncao, M.; Bermudez, V. D. Z. *J. Phys. Chem. B* **2004**, *108*, 14924.
(24) Carlos, L. D.; Ferreira, R. A. S.; Rainho, J. P.; Bermudez, V. D. Z. *Adv. Funct. Mater.* **2002**, *12*, 819.
(25) Quach, A.; Escax, V.; Nicole, L.; Goldner, P.; Guillot-Noel, O.; Aschehoug, P.; Hesemann, P.; Moreau, J.; Gourier, D.; Sanchez, C. *J. Mater. Chem.* **2007**, *17*, 2552.
(26) Wang, Q. M.; Yan, B. *J. Mater. Chem.* **2004**, *14*, 2450.
(27) Wang, Q. M.; Yan, B. *J. Photochem. Photobiol., A* **2006**, *178*, 70.
(28) Wang, Q. M.; Yan, B. *Cryst. Growth Des.* **2005**, *5*, 497.
(29) Wang, Q. M.; Yan, B. *J. Mater. Res.* **2005**, *20*, 592.
(30) Wang, Q. M.; Yan, B. *J. Photochem.Photobiol., A* **2006**, *175*, 159.
(31) Wang, Q. M.; Yan, B. *J. Organomet. Chem.* **2006**, *691*, 545.
(32) Wang, Q. M.; Yan, B. *J. Organomet. Chem.* **2006**, *691*, 3567.
(33) Yan, B.; Ma, D. J. *J. Solid State Chem.* **2006**, *179*, 2059.
(34) Yan, B.; Qiao, X. F. *Photochem. Photobiol.* **2007**, *83*, 971.
(35) Yan, B.; Wang, F. F. *J. Organomet. Chem.* **2007**, *692*, 2395.
(36) Goncalves, M.C.; Bermudez, V. D. Z.; Ferreira, R. A. S.; Carlos, L. D.; Rocha, D. J. *Chem. Mater.* **2004**, *16*, 2530.
(37) Schmider, M.; Muh, E.; Klee, J. E.; Mulhaupt, R. *Macromolecules* **2005**, *38*, 9548.
(38) Hu, D.; Croutxe-Barghorn, C.; Feuillade, M.; Carre, C. *J. Phys. Chem. B* **2005**, *109*, 15214.
(39) Peng, F.; Lu, L.; Sun, H.; Wang, Y.; Liu, J.; Jiang, Z. *Chem. Mater.* **2005**, *17*, 6790.
(40) Chang, Y.; Allcock, H. R. *Chem. Mater.* **2005**, *17*, 4449.

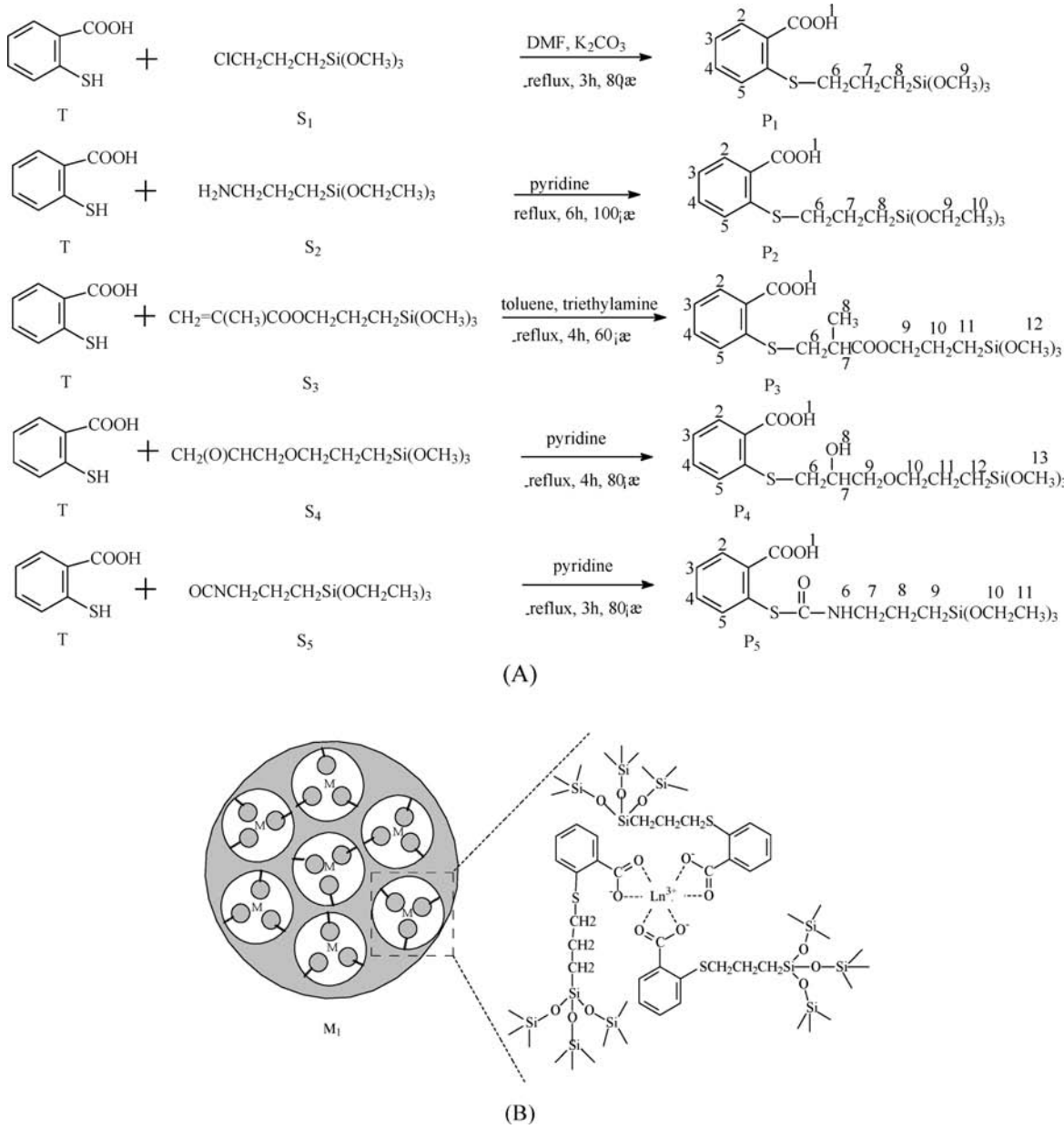

Figure 1. (A) Scheme for synthesis of five precursors on the modification of thiosalicylic acid and (B) scheme for the predicted structure of the hybrid materials.

before utilization according to the literature procedures.[41] Europium and terbium nitrates were obtained from the corresponding oxides in dilute nitric acid.

Synthesis of precursors. Five precursors were prepared according to the procedures depicted in part A of Figure 1 using thiosalicylic acid (T) as starting reagent. The modifications were performed by addition of 3-chloropropyltriethoxysilane (S_1), 3-aminopropyltrimethoxysilane (S_2), 3-methacryloyloxypropyltrimethoxysilane (S_3), 3-glycidoxypropyltrimethoxysilane (S_4), and 3-(triethoxysilyl)propyl isocyanate (S_5).

Modified by 3-Chloropropyltrimethoxysilane. Thiosalicylic acid (0.925 g, 6 mmol) was first dissolved in 15 mL *N*,*N*-dimethylformamide (DMF) by stirring and 3-chloropropyl trimethoxysilane (1.192 g, 6 mmol) was then added to the solution by drops. K_2CO_3 (0.05 g) was added as catalyzer. The whole mixture was refluxing at 80 °C for 3 hours. After filtration, the solution was then condensed to evaporate the solvent. The residue was dried on a vacuum line, and yellow oil was obtained. It was named P_1 in this article. Yield: 86 %. Anal. Calcd for $C_{13}H_{20}O_5SSi$ (%): C 49.34, H 6.37; Found: C 48.98, H 6.13. 1H NMR ($CDC1_3$, 500 MHz) 0.78(t, 2H, H_8), 1.88(m, 2H, H_7), 3.15(t, 2H, H_6), 3.58(s, 9H, H_9), 7.15 (q, 1H, H_3), 7.32(d, 1H, H_5), 7.77(q, 1H, H_4), 8.08(d, 1H, H_2), 11.0(s, 1H, H_1).

Modified by 3-Aminopropyltrimethoxysilane. Thiosalicylic acid (0.925 g, 6 mmol) was first dissolved in 15 mL pyridine by stirring and then 3-aminopropyl trimethoxysilane (1.326 g, 6 mmol) was added to the solution by drops. The whole mixture was refluxing at 100 °C for 6 hours. The solution was condensed to evaporate the solvent, and then the residue was dried on a vacuum line under argon atmosphere. A yellow oil product was obtained, and it was named P_2 in this article. Yield: 74 %. Anal. Calcd for $C_{16}H_{26}O_5Ssi$ (%): C 53.60, H 7.31; Found: C 54.02, H 7.03. 1H

(41) Lima, P.; Junior, S. A.; Malta, O. L.; Carlos, L. D.; Ferreira, R. A. S.; Pavithran, R.; Reddy, M. L. P. *Eur. J. Inorg. Chem.* **2006**, 3923.

NMR ($CDC1_3$, 500 MHz) 0.68(t, 2H, H_8), 1.28(t, 9H, H_{10}) 1.71(m, 2H, H_7), 3.14(t, 2H, H_6), 3.57(q, 6H, H_9), 7.17 (q, 1H, H_3), 7.42(d, 1H, H_5), 7.72(q, 1H, H_4), 7.95(d, 1H, H_2), 11.0(s, 1H, H_1).

Modified by 3-Methacryloyloxypropyltrimethoxysilane. Thiosalicylic acid (0.925 g, 6 mmol) was first dissolved in 15 mL toluene by stirring and then 3-methacryloyloxypropyl trimethoxysilane (1.490 g, 6 mmol) was added to the solution by drops. Three drops of triethylamine was added as catalyzer. The whole mixture was refluxing at 60 °C for 4 hours. After being condensed to evaporate the solvent and dried on a vacuum line under argon atmosphere, the solution turned to be yellow oil and it was named P_3 in this article. Yield: 71 %. Anal. Calcd for $C_{17}H_{26}O_7SSi$ (%): C 50.72, H 6.51; Found: C, 50.53, H 6.34. 1H NMR ($CDC1_3$, 500 MHz) 0.68(t, 2H, H_{11}), 1.22(d, 3H, H_8), 1.71(m, 2H, H_{10}), 2.61(m, 1H, H_7), 3.17(t, 2H, H_6), 3.74(t, 2H, H_9), 3.58(s, 9H, H_{12}), 7.17 (q, 1H, H_3), 7.34(d, 1H, H_5), 7.46(q, 1H, H_4), 8.10(d, 1H, H_2), 11.25(s, 1H, H_1).

Modified by 3-Glycidoxypropyltrimethoxysilane. Thiosalicylic acid (0.925 g, 6 mmol) was first dissolved in 15 mL pyridine by stirring and then 3-glycidoxypropyltrimethoxysilane (1.418 g, 6 mmol) was added to the solution by drops. The whole mixture was refluxing at 80 °C for 4 hours. After being condensed to evaporate the solvent and dried on a vacuum line under argon atmosphere, the solution turned to be red oil and it was named P_4 in this article. Yield: 82 %. Anal. Calcd for $C_{16}H_{26}O_7SSi$ (%) C 49.21, H 6.71; Found: C 49.40, H 6.51. 1H NMR ($CDC1_3$, 500 MHz) 0.69(t, 2H, H_{12}), 1.71(m, 2H, H_{11}), 3.14(t, 2H, H_{10}), 3.45(t, 2H, H_6), 3.57(s, 9H, H_{13}), 3.72(t, 2H, H_9), 3.85(m, 1H, H_7), 4.02(s, 1H, H_8), 7.16 (q, 1H, H_3), 7.38(d, 1H, H_5), 7.42(q, 1H, H_4), 8.02(d, 1H, H_2), 11.0(s, 1H, H_1).

Modified by 3-(Triethoxysilyl)propylisocyanate. 3-(triethoxysilyl)propyl isocyanate (1.484 g, 6 mmol) was first dissolved in 15 mL pyridine by stirring and then thiosalicylic acid (0.925 g, 6 mmol) was added to the solution by drops. The whole mixture was refluxing at 80 °C for 3 hours. After being condensed to evaporate the solvent and dried on vacuum line under argon atmosphere, yellow oil was obtained, and it was named P_5 in this article. Yield: 75 %. Anal. Calcd for $C_{17}H_{27}O_6NSSi$ (%): C 50.85, H 6.78, N 3.49; Found: C 51.08, H 6.46, N 3.31. ^{1}H NMR ($CDC1_3$, 500 MHz) 0.64(t, 2H, H_9), 1.244(t, 9H, H_{11}), 1.56(m, 2H, H_8), 3.23(t, 2H, H_7), 3.78(q, 6H, H_{10}), 7.32 (q, 1H, H_3), 7.43(t, 1H, H_6), 7.71(d, 1H, H_5), 7.90(q, 1H, H_4), 8.75(d, 1H, H_2), 11.2(s, 1H, H_1).

Synthesis of the Hybrid Materials. Sulfonamide precursor (0.6 mmol, P_1 for example) was dissolved in ethanol with stirring. Then, 0.2 mmol $Eu(NO_3)_3 \cdot 6H_2O$ and 1.2 mmol tetraethoxysilane (TEOS) was added into the solution to enhance the sol−gel process. Diluted hydrochloric acid (0.5 mL) was put into the solution to change pH to 1 to promote hydrolysis. The mixture was agitated magnetically in a covered Teflon beaker for an hour, and then the pH was adjusted to 7 with diluted hydrochloric acid (1.0 mL) for condensation. After that, it was aged at 60 °C for the gelation in 3 days. The gels were collected and ground as powder materials for the optic studies. This kind of hybrid material was named of Eu-M_1 for short. Other europium hybrids can be named as Eu-M_2, Eu-M_3, Eu-M_4, and Eu-M_5. When $Eu(NO_3)_3 \cdot 6H_2O$ was replaced by $Tb(NO_3)_3 \cdot 6H_2O$, ($Dy(NO_3)_3 \cdot 6H_2O$, and $Sm(NO_3)_3 \cdot 6H_2O$) in the reagents, another three series of hybrid materials could be prepared, which can be named of Tb-M_i (Dy-M_i, Sm-M_i, $i = 1 - 5$) (the scheme in part B of Figure 2).

Physical Properties. Fourier transform infrared (FTIR) spectra were measured within the 4000−400 cm^{-1} region on an (Nicolet Nexus 912 AO446) infrared spectrophotometer with the KBr pellet technique. ^{1}H NMR (proton nuclear magnetic resonance) spectra were recorded in $CDCl_3$ on a Bruker Avance-500 spectrometer with tetramethylsilane as an inter-reference. Elemental analyses (carbon, hydrogen, nitrogen) were determined with a Carlo Erba EA1110 elemental analyzer. Scanning electronic microscope (SEM) images were obtained with a Philips XL-30. The X-ray diffraction (XRD) measurements were carried out on powdered samples via a Bruker D8 diffractometer (40 mA, 40 kV) using monochromatic Cu Kα1 radiation ($\lambda = 1.54$ Å) over the 2θ range of 10−70°. Differential scanning calorimetry (DSC) and thermogravimetric analysis (TGA) was performed on a Netzsch STA 449C with a heating rate of 20 K/min under a nitrogen atmosphere (flow rate: 40 ml/min). Phosphorescent spectra (chloroform solution) and luminescence (excitation and emission) spectra of these solid complexes were determined with a RF-5301 spectrophotometer whose excitation and emission slits were 5 and 3 nm. All of the emission and excitation spectra were corrected, and the intensities were determined with integrated area, and the fluorescence decay properties were recorded on an Edinburgh Analytical Instruments.

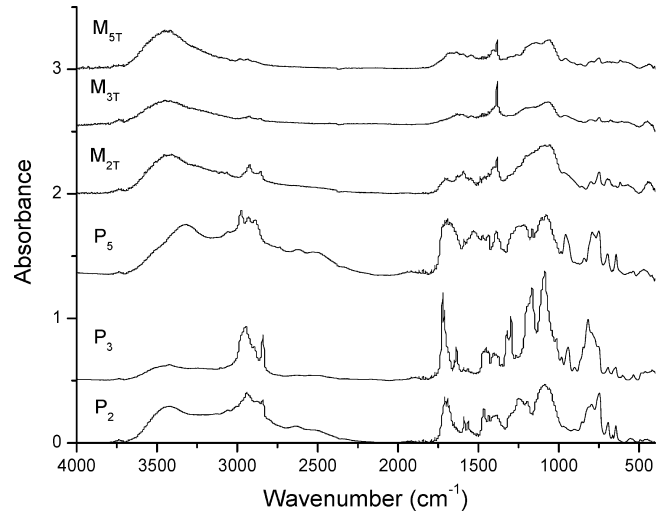

Figure 2. Selected FTIR spectra for three precursors (P_2, P_3, and P_5) and their hybrid materials (M_{2T}, M_{3T}, and M_{5T}).

Results and Discussion

Chemical Characterizations of the Functional Molecular Bridge. The FTIR spectra for selected three precursors (P_2, P_3, and P_5) and three hybrid materials (Tb-M_2, Tb-M_3, and Tb-M_5) are presented in Figure 1. The modifying reactions of thiosalicylic acid (from T to P_1, P_2, P_3, P_4, and P_5, respectively) are evidenced by the vanishing of the ν(S−H) at 2521 cm^{-1} and an increase of ν(C−S−C) at 695−655 cm^{-1} (in Figure 2).[42] The broad peak at 3064−2817 cm^{-1} in curve T is the coupling of two thiosalicylic acids' carboxyl, and it turned into broad peak of ν(O−H) at 3454 cm^{-1} in curves of five precursors. Two adjacent sharp peaks at 2952 and 2847 cm^{-1} in curves of five precursors are $\nu_{as}(CH_2)$ and $\nu_s(CH_2)$ of the long carbon chain in precursors. And ^{1}H NMR spectra relative to the precursors are in full agreement with the proposed structures. Furthermore, the spectra of hybrid materials (Tb-M_2, Tb-M_3, and Tb-M_5) are dominated by the ν(O−H) at 3454 cm^{-1} and ν(Si−O−Si) absorption bands at 1120−1000 cm^{-1}. The ν(Si−C) vibration located in the 1193 cm^{-1} in IR spectra of hybrid materials

(42) Vijaikumar, S.; Pitchumani, K. *J. Mol. Catal. A: Chem.* **2004**, *217*, 117.

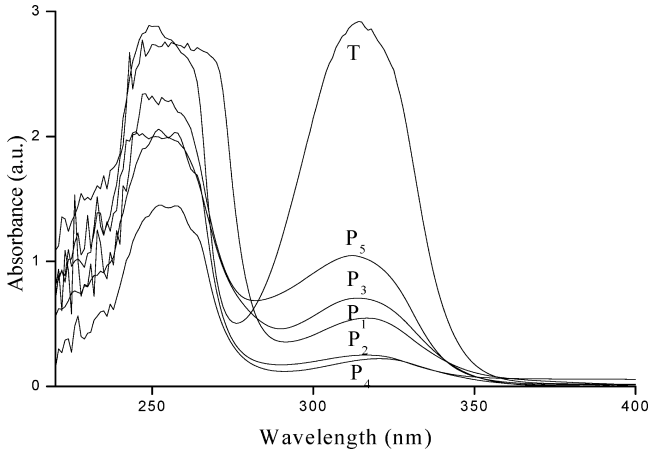

Figure 3. Ultraviolet absorption spectra of thionsalicylic acid (T) and five precursors (P_1-P_5).

(Figure1) was consistent with the fact that no (Si−C) bond cleavage occurred during the hydrolysis and condensation reactions.[20] The broad absorption band at 1120−1000 cm^{-1} (ν(Si−O−Si)) indicated the formation of siloxane bonds.[43] The decrease of other peaks' intensities may be due to the containing of the organic groups by the silicate inorganic host, which occurred in the hydrolysis and condensation process.

At the same time, the coordination reaction between Ln^{3+} ions and the ligands is also clearly shown by infrared spectroscopy. The $\nu(COO^-)_{as}$ vibrations and $\nu(COO^-)_{sy}$ are shifted to lower frequencies ($\gamma\nu$ = 40−70 cm^{-1}) after coordination to the metallic ion with the oxygen atom of the carbonyl group.[20] However, in the case of P_3 the coordination couldn't be distinguished clearly from the infrared spectroscopy because there were two (C═O) groups in one molecule, and the peak of uncoordinated (C═O) covered up the shift. In the spectra of precursors, the $\nu(COO^-)_{sy}$ vibrations is located at 1443 cm^{-1}. But in the spectrum of the hybrid materials, the $\nu(COO^-)_{sy}$ vibrations is shifted to the 1384 cm^{-1}, which is the proof of the coordination of the carboxylic group to the central ion with the oxygen atoms.

Figure 3 shows the UV absorption spectra of thionsalicylic acid (T) and five precursors (P_1-P_5). From the spectra, it can be clearly seen that the absorption at 250 nm corresponded to the $\pi \rightarrow \pi^*$ electronic transition of aromatic carboxylic acids (K strip), and the absorption at 314 nm corresponded to the $n \rightarrow \pi^*$ electronic transition of the sulfide group (R strip).[44] In addition, there was a change of molar absorbance at 314 nm from thionsalicylic acid to precursor. This indicated that the mercapto ligands have been modified because the modification decreased the probability of the noncovlent electrons.

Chemical Characterizations of the Hybrid Materials. The XRD diffractogram of the selected europium hybrid materials reproduced in Figure 4. The hybrid materials are

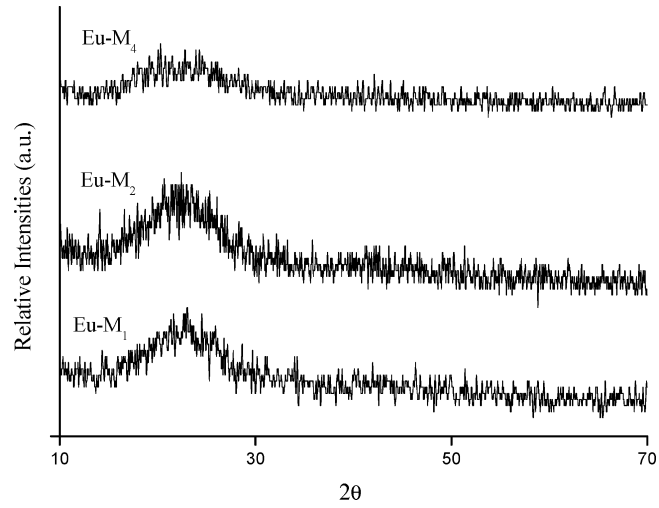

Figure 4. X-ray diffraction (XRD) graphs of the hybrid material.

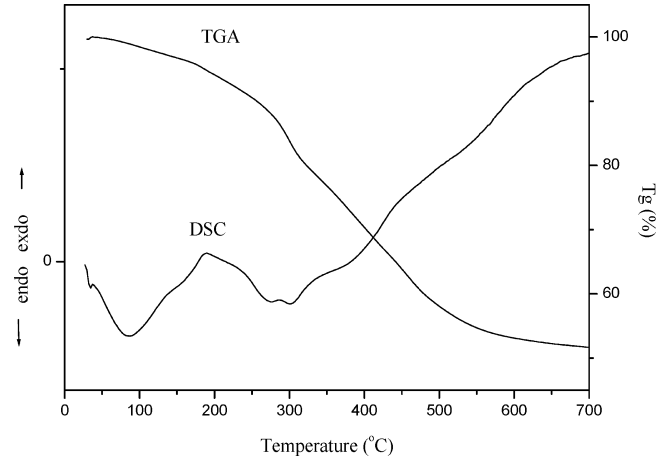

Figure 5. DSC and TGA traces of Eu-M_1 hybrid material.

totally amorphous in the range of 10° ≤ n ≤ 70°. Broad signals are observed and it is well-known that these broad signals correspond to the existence of a short-range order in the material.[45] The broad peaks centered on 23.02 ° for Eu-M_1 and 22.80 ° for Eu-M_2 in the XRD patterns of the material were ascribed to the coherent diffraction of the siliceous backbone of the hybrids.[46,47] The absence of any crystalline regions in these samples correlates well with the presence of organic chains in the host inorganic framework. These phenomena lead us to conclude that neither free europium/terbium nitrates salt, pure crystalline thiosalicylic acid, nor crystalline lanthanide complexes occurs throughout the range of those materials.

Figure 5 shows the DSC and TGA traces of Eu-M_1. In curve of DSC, there are two endothermic peaks. The first one, from 40 °C to 187 °C, is due to the loss of the coordinated H_2O.[47] The mass loss of 4.0 % for this thermal event is revealed by the TGA curve, and it was calculated

(43) Perrin, D. D.; Armarego, W. L. F.; Perrin, D. R. *Purification of Laboratory Chemicals*; Pergamon Press: Oxford, U.K., 1980.
(44) Pretsch, E.; Buhlmann, P.; Affolter, C. *Structure Determination of Organic Compounds*, 2nd ed.; Springer: Berlin, 2003.
(45) Cerveau, G.; Corriu, R. J. P.; Framery, E.; Lerouge, F. *Chem. Mater.* **2004**, *16*, 3794.
(46) Carlors, L. D.; Bermudez, V. D. Z.; Ferreira, R. A. S.; Marques, L.; Assuncao, M. *Chem. Mater.* **1999**, *11*, 581.
(47) Nobre, S. S.; Lima, P. P.; Mafra, L.; Ferreira, R A. S.; Freire, R. O.; Fu, L. S.; Pischel, U.; Bermudez, V. D.; Malta, O. L.; Carlos, L. D. *J. Phys. Chem. C* **2007**, *111*, 3275.

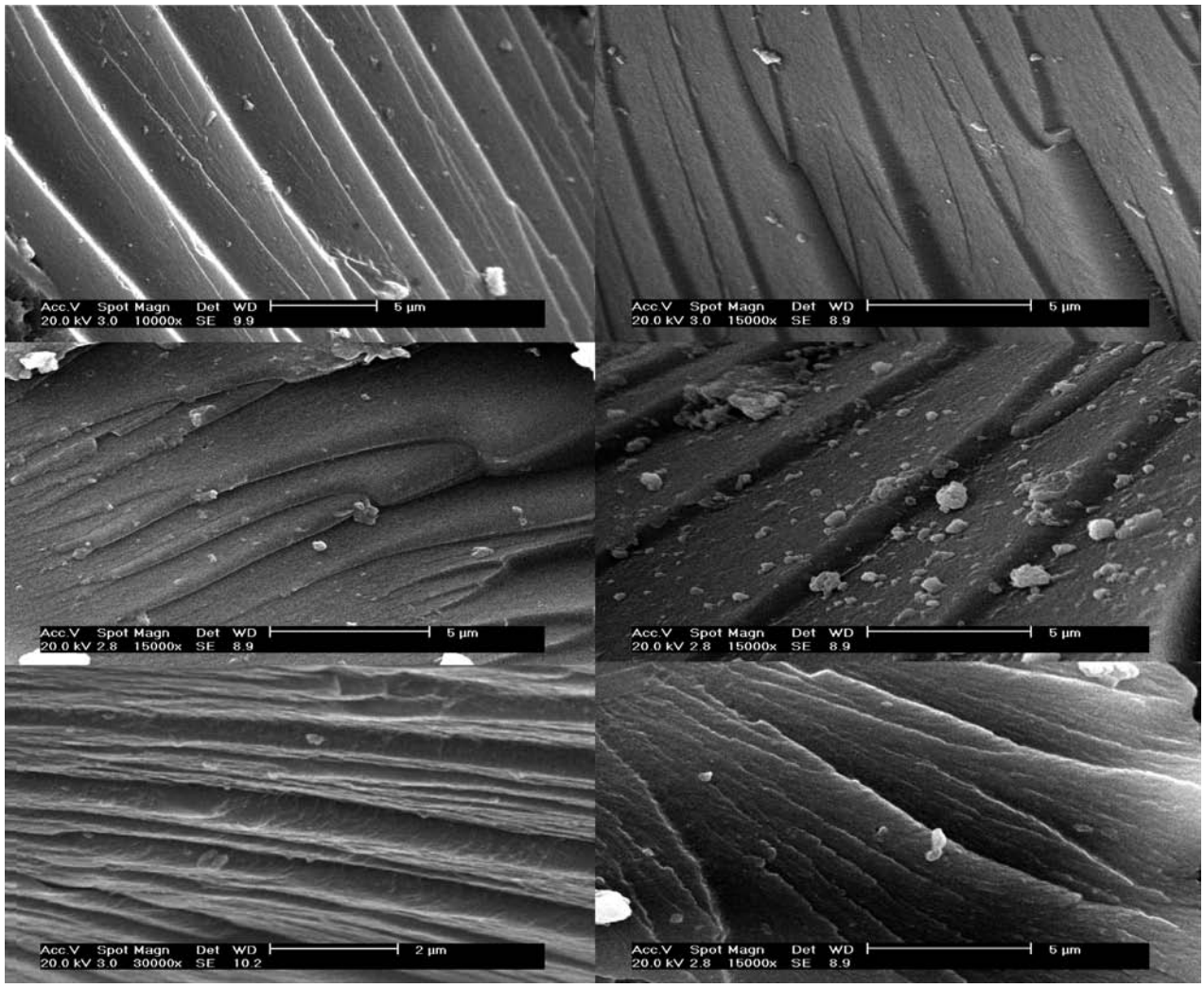

Figure 6. Scanning electron micrograph (SEM) for the hybrid materials.

that there are approximately three molecular H_2O in one complex. The second peak, which ranges from 187 °C to 400 °C, is the decomposition of the materials. The total mass loss up to 700 °C is 48.3 %, which slightly disagrees with the theoretical value 47.9 % calculated by taking the inorganic parts as the final products. The excrescent loss is attributed to the adsorption water on the materials' amorphous surface. Generally, the thermal stability of the polymer hybrid is higher compared with that of the pure polymer or complexes. It is assumed that the rigid silica matrix surrounds the organic polymer by molecular level hybridization.[4–7] Although the thermal stability of this kind of hybrid was better than that of pure complex,[48] it is still lower in this article. As shown in Figure 5, the organic parts decompose even at 200 °C. This defect in thermal stability can be explained by the thermal instability of the organic parts. But in view of the actual application temperature, these hybrid materials are still useful in many areas. According to the previous section and other references,[49,50] a 9-fold coordination involving 6 oxygen atoms of carboxylic groups and 3 oxygen atoms of water molecular could be supposed for Ln^{3+} ions. The resulting predicted complex structure of one hybrid material is presented as an example in Figure 2. Because the precursors had big organic groups and long chairs, there were some difficulties to make them extend in one direction, and especially for that the hybrid materials made from siloxane by sol−gel process were amorphous; the actual atom configurations may be slightly distorted against the predicted structure.

The scanning electron micrographs (SEM) of the representative lanthanide hybrid materials demonstrate that a skin-wrinkling material was obtained (Figure 6, in the order: Eu-M_1, Eu-M_2, Eu-M_3, Eu-M_4, Eu-M_5, Tb-M_5). On the surface of those materials, there are many linear stripes, which are mostly owing to the sol−gel treatment. In the gelation process, rudimental solutions were released from the inside of the gel. Because the foundation shrinks homogeneously, the skin of the material takes on a regular morphology. It is also a proof that no phase separation occurred. All of the functional molecular bridges derive from the sulfide of T with P_1-P_5 and the carboxylate group is kept, so the coordination behavior mainly depends on the carboxylate group. As we know, lanthanide complexes of carboxylate

(48) Shen, X. Q.; Qiao, H. B.; Li, Z. J. *Inorg. Chim. Acta* **2006**, *359*, 642.
(49) Yin, M. C.; Yuan, L. J.; Ai, C. C. *Polyhedron* **2004**, *23*, 529.
(50) Yan, B.; Song, Y. S.; Chen, Z. X. *J. Mol. Struct.* **2004**, *694*, 115.

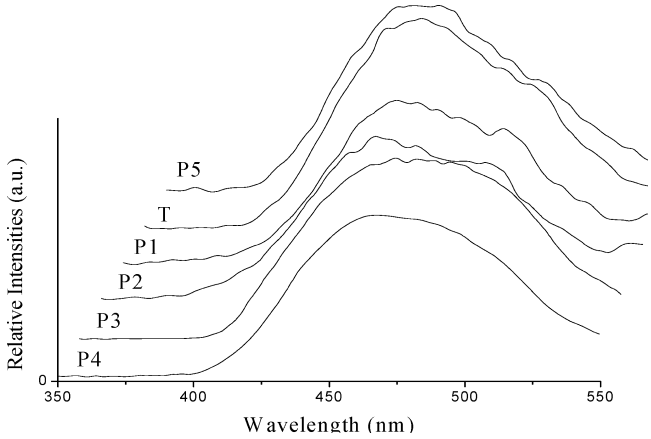

Figure 7. Phosphorescence spectra of thiosalicylic acid (T) and five precursors (P_1-P_5).

derivatives readily form the polymeric structure, and the carboxlate groups possess the bridging coordination ability. This tendency will compete with the construction of a polymeric network structure of Si−O−Si in the hydrolysis and copolycondensation processes of silica. Finally, these hybrid materials retain the intensive tendency of growing into a polymeric microstructure and reserve the coordinated positions in the corresponding bulk materials observed from the microstructure view in Figure 6. Different hybrids derived from different sulfide linkages only have a little influence on the micromorphology, and the terbium hybrids show the similar microstructure and here only show the example of Tb-M5, suggesting the lanthanide ions hardly affect the microstructure in these hybrids.

Photophysical Properties. Aromatic carboxylic acids are already well-known to be good chelating groups to sensitize luminescence of lanthanide ions.[4] The mechanism usually described for sensitized emission in lanthanide complexes proceeds through the following steps. At first, the ligands absorb energy via a ground singlet-excited singlet transition. Then, the energy is transferred from the excited singlet to the triplet state through an intersystem crossing process. After ligands transfer energy to excited metal ion states, the emission from the lanthanide ions' excited state will be observed.[20]

The low-temperature phosphorescence spectra of thiosalicylic acid (T) and five precursors (P_1-P_5) are recorded in Figure 7. All of the curves exhibited a broad phosphorescence band which corresponds to the triplet state emission of the ligands.[20] The red shift as above was observed between T and precursors except for P_1-P_5, suggesting conjugate groups have been modified for the coordination reaction. The energy differences (ΔE) between the triplet state energy levels and the resonant emissive energy levels of Ln^{3+} (Ln = Eu, Tb, Dy, Sm) were taken at the maximum of emission and are reported in Table 1. According to the energy transfer and intramolecular energy mechanism,[51–55] the intramolecular energy migration efficiency from organic ligands to the central Ln^{3+} is the most important factor to determine the luminescence properties of lanthanide complexes.[54] The intramolecular energy transfer efficiency is established mainly on two energy transfer processes.[55] One is from the triplet state energy of organic ligands to the resonant energy level by Dexter's resonant exchange interaction theory:[47]

$$k_{ET}=KP_{da}\exp(-2R_{da}/L) \quad (1)$$

$$P_{da}=(2\pi Z^2/R)\int F_d(E)E_a(E)dE \quad (2)$$

$$k_{ET}=KP_{da}\exp(-2R_{da}/L)=K'F_d(E)E_a(E)dE \quad (3)$$

The other is the inverse energy transition by thermal deactivation mechanism[48]

$$k(T)=A\exp(-\Delta E/RT) \quad (4)$$

k_{ET} is the rate constant of the intramolecular energy transfer, and P_{da} is the transition probability by the resonant exchange interaction. $2\pi Z^2/R$ is a constant relative to the specific mutual distance between the central Ln^{3+} ion and its coordinated atoms (oxygen or nitrogen). $F_d(E)$ and $E_a(E)$ are the experimental luminescence spectrum of energy donor (ligands) and the experimental absorption spectrum of energy acceptor (Ln^{3+}), respectively, so both of them represent the overlap spectrum of Ln^{3+} cations. R_{da} is the intramolecular distance between donor atoms and acceptor atoms, and L is the van der Waals radius. Both R_{da} and L may be considered to be constant in intramolecular transfer processes, so k_{ET} is proportional to the overlap of $F_d(E)$ and $E_a(E)$. With the decrease of the energy difference between the triplet state of conjugated carboxylic acid and Ln^{3+} excited levels, the overlap of $F_d(E)$ and $E_a(E)$ is increased. So, from eq 6, it can be concluded that the more the overlap between the luminescence spectrum of organic ligands and the excited state energy levels of Ln^{3+} ions, the more the intramolecular energy rate constant k_{ET}. On the other hand, the activation energy ΔE in eq 7 is equal to the energy difference ΔE (Tr-Ln^{3+}), whereas from the formula the inverse energy transfer rate constant $k(T)$ increased with decreasing ΔE (Tr-Ln^{3+}).[52,53] As discussed above, there should exist an optimal energy difference between the triplet state position of organic ligands and the emissive energy level of Ln^{3+} ions, the larger for eq 6 and the smaller for eq 7 ΔE (Tr-Ln^{3+}) will decrease the luminescence properties of lanthanide complexes. In consequence, the energy level differences between the triplet state energy of Cali-Si (24 630 cm^{-1}) and the resonant emitting levels of Tb^{3+} (20 500 cm^{-1}) or Eu^{3+} (17 265 cm^{-1}) are 4130 and 7365 cm^{-1}, respectively, suggesting that the specific energy transfer mechanism is more favorable for Tb^{3+} than for Eu^{3+} ions. The following emission spectra obtained from terbium and europium hybrids further demonstrate our predicted conclusion.

Figure 8 gives the excitation spectra of the resulting selected europium hybrid materials monitored at 614 nm, which exhibit a broad excitation band centered at 360 nm in the long-wavelength UV range, which can be ascribed the

(51) Sato, S.; Wada, M. *Bull. Chem. Soc. Jap.* **1970**, *43*, 1955.
(52) Dexter, D. L. *J. Chem. Phys.* **1953**, *21*, 836.
(53) Dean, C. R. S.; Shepherd, T. M. *J. Chem. Soc., Faraday Trans. 2* **1975**, *71*, 146.
(54) Wang, Q. M.; Yan, B.; Zhang, X. H. *J. Photochem. Photobiol., A.* **2005**, *174*, 119.
(55) Yan, B.; Zhou, B. *J. Photochem. Photobiol., A.* **2005**, *171*, 181.

Table 1. Triplet-State Energies of Molecular Bridges and Their Energy Transfer with Lanthanide Ions

	λ_{max} (nm)	triplet-state energies (cm^{-1})	$\Delta E(Tr\text{-}Eu^{3+})$ (cm^{-1})	$\Delta E(Tr\text{-}Tb^{3+})$ (cm^{-1})	$\Delta E(Tr\text{-}Dy^{3+})$ (cm^{-1})	$\Delta E(Tr\text{-}Sm^{3+})$ (cm^{-1})
T	448	22 320	5020	1820	1320	4420
P_1	458	21 835	4535	1335	835	3935
P_2	458	21 835	4535	1335	835	3935
P_3	473	21 140	3840	640	140	3240
P_4	469	21 320	4020	820	320	3420
P_5	439	22 780	5480	2280	1780	4880

charge transfer state (CTS) of Eu−O.[56,57] The strong CTS absorption is favorable for the efficient energy migration of Eu^{3+}, and the effective luminescence of Eu^{3+} can be expected. Besides, weak absorption bands in the range of the short wavelength ultraviolet region of 200−250 nm occur, corresponding to the host absorption of the Si−O network. No f−f transitions could be observed in the spectra (they are too weak). All of the other lanthanide hybrid materials have similar excitation spectra.

The luminescence behaviors of all of the materials have been investigated at 298 K by direct excitation of the ligands (360 nm). Representative emission spectra are given in Figures 9 and 10, and the detailed luminescent data are shown in Tables 2 and 3. There are narrow-width red emissions of europium hybrid materials. The narrow-width

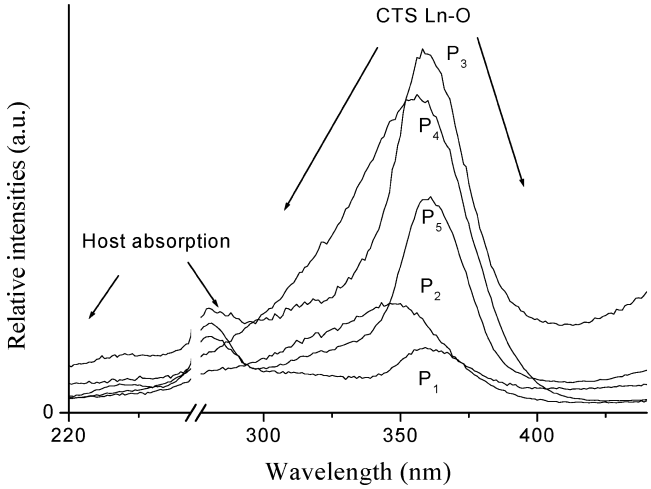

Figure 8. Selected excitation spectra of the europium hybrid materials.

Table 2. Luminescence Efficiencies and Lifetimes of the Europium Covalent Hybrids

systems	$Eu\text{-}M_1$	$Eu\text{-}M_2$	$Eu\text{-}M_3$	$Eu\text{-}M_4$	$Eu\text{-}M_5$
υ_{00} (cm^{-1})[a]	17 331	17 331	17 331	17 331	17 331
υ_{01} (cm^{-1})[a]	16 949	16 949	16 978	16 978	16 978
υ_{02} (cm^{-1})[a]	16 287	16 340	16 313	16 260	16 313
υ_{03} (cm^{-1})[a]	15 408	15 385	15 408	15 361	15 385
υ_{04} (cm^{-1})[a]	14 347	14 347	14 347	14 306	14 347
I_{00}[b]	2.13	1.6	1.49	2.02	0.92
I_{01}[b]	45.19	50.68	27.30	31.10	15.74
I_{02}[b]	148.89	127.69	84.55	69.81	37.68
I_{03}[b]	0.99	0.50	0.69	1.03	0.42
I_{04}[b]	1.09	0.54	0.66	1.03	0.36
I_{02} / I_{01}	3.29	2.52	3.10	2.24	2.39
A_{00} (s^{-1})	2.31	1.55	2.67	3.18	2.85
A_{01} (s^{-1})	50	50	50	50	50
A_{02} (s^{-1})	171.43	130.67	161.17	117.19	124.57
A_{03} (s^{-1})	1.21	0.55	1.38	1.83	1.46
A_{04} (s^{-1})	1.42	0.63	1.43	1.97	1.35
τ (ms)[c]	0.92	0.83	0.86	0.67	0.63
A_{rad} (s^{-1})	226.37	183.04	216.65	174.17	180.23
τ_{exp}^{-1} (s^{-1})	1086.96	1204.82	1162.79	1492.54	1587.30
A_{nrad} (s^{-1})	860.59	1021.78	946.14	1318.37	1407.07
η (%)	20.8	15.2	18.6	11.7	11.3
n_w	∼1	∼1	∼1	∼1.5	∼1.5
Ω_2 ($\times 10^{-20}$ cm^2)	5.00	3.81	4.68	3.40	3.61
Ω_4 ($\times 10^{-20}$ cm^2)	0.095	0.042	0.096	0.11	0.090

[a] Energies of the $^5D_0 \rightarrow {}^7F_J$ transitions (υ_{0J}). [b] Integrated intensity of the $^5D_0 \rightarrow {}^7F_J$ emission curves. [c] For $^5D_0 \rightarrow {}^7F_2$ transition of Eu^{3+}.

green emissions are observed in the terbium hybrid materials. Figure 9 illustrates the typical photoluminescence spectra of the europium hybrid materials. The maxima of these bands are around 590 and 613 nm, associated with $^5D_0 \rightarrow {}^7F_1$ and $^5D_0 \rightarrow {}^7F_2$ transitions, respectively. A prominent feature that may be noted in these spectra is the very high intensity of the $^5D_0 \rightarrow {}^7F_2$ transition. The $^5D_0 \rightarrow {}^7F_1$ transition is a magnetic-dipolar transition and is insensitive to the local structure environment, whereas the $^5D_0 \rightarrow {}^7F_2$ transition is an

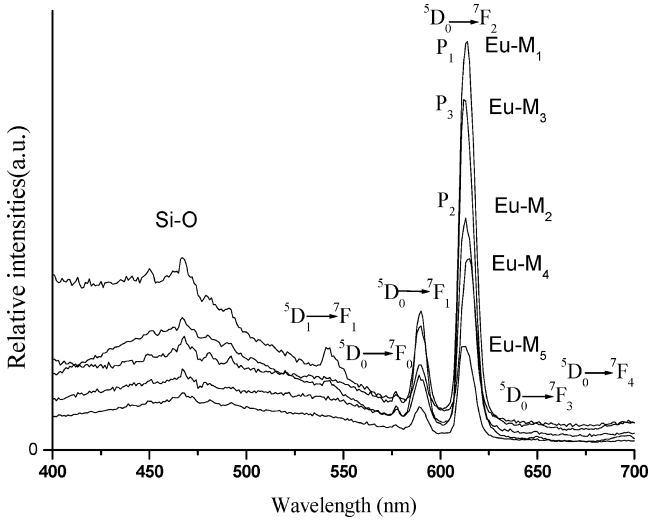

Figure 9. Emission spectra of europium hybrid materials.

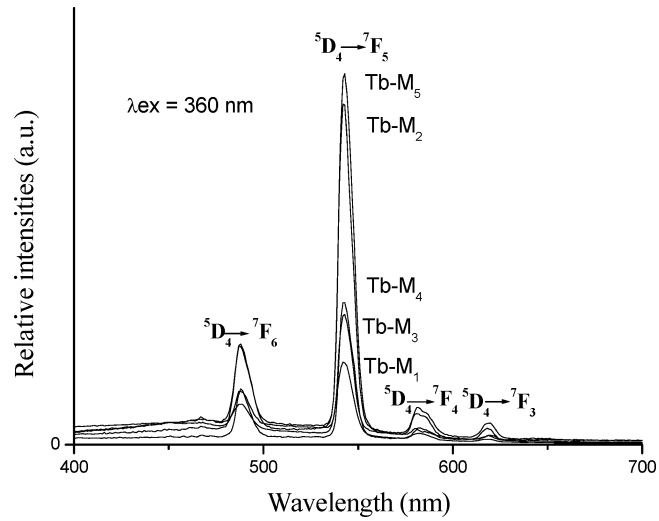

Figure 10. Emission spectra of terbium hybrid materials.

Table 3. Luminescence Data of the Terbium, Dysprosium, and Samarium Covalent Hybrid Materials

systems	Tb-M_1	Tb-M_2	Tb-M_3	Tb-M_4	Tb-M_5
τ (ms)[d]	0.95	1.09	0.93	1.08	1.21
emisson bands	487, 542, 582, 618	488, 543, 581, 620	488, 543, 583, 619	488, 543, 582, 620	488, 542, 581, 618
systems	Dy-M_1	Dy-M_2	Dy-M_3	Dy-M_4	Dy-M_5
	482, 572	482, 573	483, 573	482, 574	483, 574
systems	Sm-M_1	Sm-M_2	Sm-M_3	Sm-M_4	Sm-M_5
	597	597	597	597	597

electric-dipolar transition and is sensitive to the coordination environment of the Eu^{3+} ion. When the interactions of the rare-earth complex with its local chemical environment are stronger, the complex becomes more nonsymmetrical, and the intensity of the electric-dipolar transitions becomes more intense. As a result, the intensity (the integration of the luminescent band) ratio of the $^5D_0 \rightarrow {}^7F_2$ transition to the $^5D_0 \rightarrow {}^7F_1$ transition has been widely used as an indicator of Eu^{3+} site symmetry.[58] In these europium hybrid materials, from M_1 to M_5, the intensity ratios $I_{02}(^5D_0 \rightarrow {}^7F_2)/I_{01}(^5D_0 \rightarrow {}^7F_1)$ are 3.30, 2.52, 3.10, 2.25, and 2.39 respectively. This ratio is only possible when the europium ion does not occupy a site with inversion symmetry.[56] These data reflect the actual coordination environment of the Eu^{3+} and interpret the predicted structure above (Figure 2).

Figure 10 illustrates typical photoluminescence spectra of the terbium hybrid materials. Narrow-width emission bands with maxima at 487, 543, 580, and 619 nm are recorded. These bands are attributed to the $^5D_4 \rightarrow {}^7F_6$, $^5D_4 \rightarrow {}^7F_5$, $^5D_4 \rightarrow {}^7F_4$, and $^5D_4 \rightarrow {}^7F_3$ transitions of Tb^{3+} ions, respectively. Because these materials have a broad excited band centered at 360 nm (Figure 6) and can be excited by high-pressure mercury vapor, which has a broad emission band at 360 nm. The efficiency, thermal quenching, and life time (maintenance) will be studied in the following research before these materials are put into applications. With regard to dysprosium hybrids presenting $^4F_{9/2} \rightarrow {}^6H_J$ ($J = {}^{15}/_2$, ${}^{13}/_2$) transitions around 482 nm and 573 nm (part A of Figure 11), which can be ascribed to Dy^{3+}, were obtained especially when the blue emission ($^4F_{9/2} \rightarrow {}^6H_{15/2}$) was relatively strong. For samarium molecular hybrids, there is an apparent orange emission peak with a maximum emission wavelengths of around 597 nm (part B of Figure 11), corresponding to the characteristic emission $^4G_{5/2} \rightarrow {}^6H_{7/2}$ transitions of the Sm^{3+} ion. Dysprosium and samarium, and especially samarium hybrids, present weak luminescence, which may be due to some internal energy levels between the transitions of the two ions, resulting in the serious nonradiative loss process. Of course, the unsuitable energy match in their systems is another important reason.

The typical decay curve of the europium and terbium hybrid materials were measured, and they can be described as a single exponential ($\mathrm{Ln}(S(t)/S_0) = -k_1 t = -t/\tau$), indicating that all Eu^{3+} and Tb^{3+} ions occupy the same average coordination environment. The resulting lifetime data of europium and hybrids were given in Table 1. Further, we selectively determined the emission quantum efficiencies of the $^5D_0$ excited state of the europium ion for Eu^{3+} hybrids on the basis of the emission spectra and lifetimes of the $^5D_0$ emitting level, and the detailed luminescent data were shown in Table 1. The quantum efficiency of the luminescence step, η expresses how well the radiative processes (characterized by rate constant A_r), competes with nonradiative processes (overall rate constant A_{nr}).[59–67]

$$\eta = A_f/(A_r + A_{nr}) \tag{5}$$

Nonradiative processes influence the experimental luminescence lifetime by the equation:[59–67]

$$\tau_{exp} = (A_r + A_{nr})^{-1} \tag{6}$$

So, quantum efficiency can be calculated from radiative-transition rate constant and experimental luminescence lifetime from the following equation:[59–67]

$$\eta = A_r \tau_{exp} \tag{7}$$

where A_r can be obtained by summing over the radiative rates A_{0J} for each $^5D_0 \rightarrow {}^7F_J$ transitions of Eu^{3+}.

$$A_r = \sum A_0 J = A_{00} + A_{01} + A_{02} + A_{03} + A_{04} \tag{8}$$

The branching ratio for the $^5D_0 \rightarrow {}^7F_{5,\,6}$ transitions can be neglected as they both are not detected experimentally, whose influence can be ignored in the depopulation of the $^5D_0$ excited state.[59–67] Since $^5D_0 \rightarrow {}^7F_1$ belongs to the isolated magnetic dipole transition, it is practically independent of the chemical environments around the Eu^{3+} ion, and thus can be considered as an internal reference for the whole spectrum, the experimental coefficients of spontaneous emission, A_{0J} can be calculated according to the equation.[59–67]

$$A_{0J} = A_{01}(I_0/I_{01})(\nu_{01}/\nu_{0J}) \tag{9}$$

Here, A_{0J} is the experimental coefficient of spontaneous emissions, among A_{01} is the Einstein's coefficient of spontaneous emission between the $^5D_0$ and $^7F_1$ energy levels. In a vacuum, A_{01} as a value of 14.65 s^{-1}, when an average index of refraction n equal to 1.506 was considered, the value of A_{01} can be determined to be 50 s^{-1} approximately ($A_{01} = n^3 A_{01\ (vacuum)}$).[60,67] I is the emission intensity and can be taken

(56) Wang, Z.; Wang, J.; Zhang, H. J. *Mater. Chem. Phys.* **2004**, *87*, 44.
(57) Binnemans, K.; Lenaerts, P.; Driesen, K.; Gorller-Walrand, C. *J. Mater. Chem.* **2004**, *14*, 191.
(58) Malta, O. L.; Brito, H. F.; Menezes, J. F. S.; Silva, F. R. G. E.; Alves, S.; Farias, F. S.; deAndrade, A. V. M. *J. Lumin.* **1997**, *75*, 255.
(59) Werts, M. H. V.; Jukes, R. T. F.; Verhoeven, J. W. *Phys. Chem. Chem. Phys.* **2002**, *4*, 1542.
(60) Li, Y.; Yan, B.; Yang, H. *J. Phys. Chem. C* **2008**, *112*, 3959.
(61) Carlos, L. D.; Messaddeq, Y.; Brito, H. F.; Ferreira, R. A. S.; Bermudez, V. D.Z.; Ribeiro, S. J. L. *Adv. Mater.* **2000**, *12*, 594.
(62) Soares-Santos, P. C. R.; Nogueira, H. I. S.; Felix, V.; Drew, M. G. B.; Ferreira, R. A. S.; Carlos, L. D.; Trindade, T. *Chem. Mater.* **2003**, *15*, 100.
(63) Teotonio, E. E. S.; Espinola, J. G. P.; Brito, H. F.; Malta, O. L.; Oliveria, S. F.; de Faria, D. L. A.; Izumi, C. M. S. *Polyhedron* **2002**, *21*, 1837.
(64) Ribeiro, S. J. L.; Dahmouche, K.; Ribeiro, C. A.; Santilli, C. V.; Pulcinelli, S. H. J. *J. Sol-Gel Sci. Technol.* **1998**, *13*, 427.
(65) Malta, O. L.; dosSantos, M. A. C.; Thompson, L. C.; Ito, N. K. *J. Lumin.* **1996**, *69*, 77.
(66) de Sa, G. F.; Malta, O. L.; Donega, C. D.; Simas, A. M.; Longo, R. L.; Santa-Cruz, P. A.; da Silva, E. F. *Coord. Chem. Rev.* **2000**, *196*, 165.
(67) Boyer, J. C.; Vetrone, F.; Capobianco, J. A.; Speghini, A.; Bettinelli, M. *J. Phys. Chem. B* **2004**, *108*, 20137.

as the integrated intensity of the $^5D_0 \rightarrow {}^7F_J$ emission bands.[66,67] v_{0J} refers to the energy barycenter and can be determined from the emission bands of Eu^{3+}'s $^5D_0 \rightarrow {}^7F_J$ emission transitions. Here, the emission intensity, I, taken as integrated intensity S of the $^5D_0 \rightarrow {}^7F_{0-4}$ emission curves, can be defined as below:

$$I_{i-j} = h\omega_{i-j}A_{i-j}N_i \approx S_{i-j} \quad (10)$$

where i and j are the initial ($^5D_0$) and final levels ($^7F_{0-4}$), respectively, ω_{i-j} is the transition energy, A_{i-j} is the Einstein's coefficient of spontaneous emission, and N_i is the population of the $^5D_0$ emitting level. On the basis of the above discussion, the quantum efficiencies of the five kinds of europium polymeric hybrid materials can be determined in the order: Eu-M_1 > Eu-M_3 > Eu-M_2 > Eu-M_4 > Eu-M_5, which take agreement with the order of lifetimes. From the equation of η, it can be seen the value η mainly depends on two quantum values: one is lifetimes and the other is I_{02}/I_{01} (red/orange ratio). If the lifetimes and red/orange ratio are large, the quantum efficiency must be high. So, the different composition of the hybrid materials may have an influence on the luminescent lifetimes and quantum efficiencies.

Furtherly, we determined the Judd−Ofelt Parameters for the three covalently bonded europium hybrid materials. The spontaneous emission probability, A, of the transition is related to its dipole strength according to eq 7.[66–69]

$$A = (64\pi^4\nu^3)/[3h(2J+1)]\{[(n^2+2)^2/9n]S_{(ED)} + n^2S_{(MD)}\} \quad (11)$$

υ is the average transition energy in cm^{-1}, h is Planck constant, $2J + 1$ is the degeneracy of the initial state (1 for $^5D_0$), and $S_{(ED)}$ and $S_{(MD)}$ are the electric and magnetic dipole strengths, respectively. The factors containing the medium's refractive index n result from local field corrections that convert the external electromagnetic field into an effective field at the location of the active center in the dielectric medium. Among all of the transitions from $^5D_0$ to $^7F_{0,3,5}$ ($J = 0, 3, 5$) are forbidden both in magnetic and induced electric dipole schemes ($S_{(ED)}$ and $S_{(MD)}$ are zero). The transition from $^5D_0$ to to $^7F_1$ ($J = 1$) is the isolated magnetic dipole transition and has no electric dipole contribution, which is practically independent of the ion's chemical environment and can be used as a reference as mentioned above.[66] Besides, the $^5D_0 \rightarrow {}^7F_6$ transition could not be experimentally detected, and it is not necessary to determine its J−O parameter. So, we only need to estimate the two parameters (Ω_2, Ω_4) related to the two purely induced electric dipole transitions $^5D_0 \rightarrow {}^7F_{2,4}$ on basis of only three parameters Ω_λ using eq 8,[67–69]

$$A = (64e^2\pi^4\nu^3)/[3h(2J+1)]\{[(n^2+2)^2/9n]\sum \Omega_\lambda |\langle J\|U^{(\lambda)}\|J'\rangle|^2 \quad (12)$$

where e is the electronic charge. With the refraction index $n = 1.506$,[67,68] and $|\langle J\|U^{(\lambda)}\|J'\rangle|^2$ values are the square reduced matrix elements whose values are 0.0032 and 0.0023 for $J = 2$ and 4,[69,70] respectively. The Ω_2, Ω_4 intensity parameters for the three hybrid materials are shown in Table 1. The distinction of the two intensity parameters for the three hybrids is not apparent, suggesting that the Eu^{3+} ion is located in a polarizable chemical environment for luminescence. It is worthy to point out that Eu-M_1 and Eu-M_3 hybrids possess higher covalency. The deep relationship between the different hybrid materials and the luminescent behavior needs to be fundamentally investigated further.

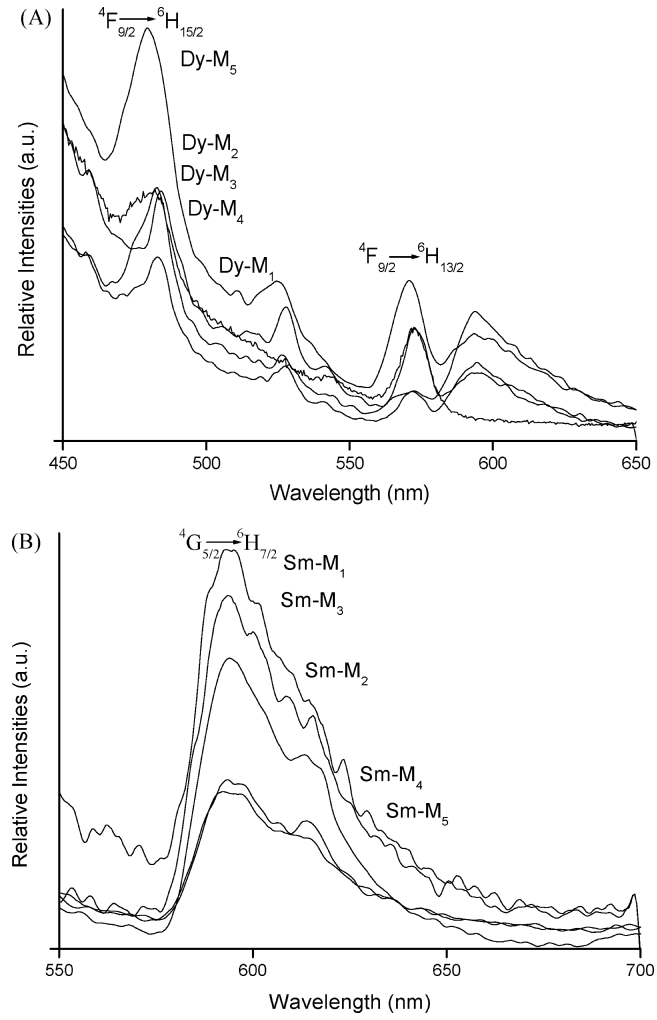

Figure 11. Emission spectra of dysprosium (A) and samarium (B) hybrid materials.

To study the coordination environment surrounding lanthanide ions, especially the influence caused by vibrations of water molecules, according to Horrocks' previous research,[70,71] it is therefore expected that probable number of coordinated water molecules (η_w) can be calculated as following equation:

$$\eta_w = 1.05(A_{exp} - A_{rad}) \quad (13)$$

On the basis of the results, the coordination number of water molecules (europium-containing hybrid materials) can be estimated to be 1−2. The coordination water molecules produce the severe vibration of the hydroxyl group, resulting

(68) Kodaira, C. A.; Claudia, A.; Brito, H. F.; Felinto, M. C. F. C. *J. Solid State Chem.* **2003**, *171*, 401.
(69) Binnemans, K.; Van Herck, K.; Gorller-Walrand, C. *Chem. Phys. Lett.* **1997**, *266*, 297.

in the large nonradiative transition and decreasing the luminescent efficiency.

Conclusions

In summary, a series of luminescent lanthanide hybrid molecular-based materials were achieved using the thiosalicylic acid derivative precursors. The different functional molecular bridges have some influence on the microstructure, especially on the photophysical properties such as luminescent lifetimes and quantum efficiencies. Furthermore, the current molecular design method can be conveniently applied to other hybrid systems. The desired properties can be tailored by an appropriate choice of the precursors. So, this kind of molecular-based hybrid material can be expected to be a promising candidate for tailoring desired properties to the host in many fields of applications.

Note Added after ASAP Publication. Figure 1 was modified from the version published ASAP May 28, 2008; the corrected version published ASAP May 30, 2008.

Acknowledgment. This work was supported by the National Natural Science Foundation of China (grant 20671072).

IC7021825

(70) Horrocks, W.; De, W.; Sudnick, D. R. *J. Am. Chem. Soc.* **1979**, *101*, 334.

(71) Horrocks, W.; De, W.; Sudnick, D. R. *Acc. Chem. Res.* **1981**, *14*, 384.